Comparison of Constant Strain Triangular and Allman Triangular Membrane Elements in Plate Structural Analysis by Finite Element Method

Piyamabhorn Uttamung[1], Pichayen Bhothikhun[2], Atipong Malatip[1] and Somboon Otarawanna[1,*]

[1] National Metal and Materials Technology Center (MTEC), 114 Thailand Science Park, Paholyothin Rd., Klong 1, Klong Luang, Pathumthani 12120

[2] Department of Mechanical Engineering, Faculty of Engineering, Chulalongkorn University, Phayathai Rd., Patumwan, Bangkok 10330

*Corresponding Author: somboono@mtec.or.th, Tel.: 02 564 6500 ext. 4320, fax: 02 564 6370

Abstract

The so-called flat shell triangular element is commonly used for plate structural analysis by finite element method (FEM). This element type is a combination of membrane and plate bending elements for plane stress and plate bending problems, respectively. Without any special treatment, solving plate structural problems by this approach leads to a numerical singularity problem due to the lack of in-plane rotation variable. The constant strain triangular (CST) element deals with the singularity difficulties by assuming a fictitious rotational stiffness. On the other hand, the Allman triangular (AT) element includes an in-plane rotational degree of freedom to avoid the singularity problem. In this study, both membrane elements were combined with the Discrete Kirchhoff triangular (DKT) plate bending element to solve plate structural problems. The performances of the two element combinations have been evaluated by several numerical examples. The numerical solutions obtained from both of the element combinations are in agreement with exact solutions when FEM mesh used is sufficiently fine. However, the AT and DKT element combination could suffer membrane locking problem in some cases when using relatively coarse mesh.

***Keywords**:* Plate structural analysis; Finite element; Flat shell triangular element; Constant strain triangle; Allman triangle

1. Introduction

In plate structural analysis by finite element method (FEM), the derivation based on shell element involves the complexity and complications in computing the element curvature. Therefore, another approach based on the assemblage of flat-faced elements, i.e. the so-called flat shell triangular element, has been widely employed [1]. This element type is a combination of membrane and plate bending elements which are commonly used in plane stress and plate bending analyses, respectively.

Membrane element contains two in-plane translational degrees of freedom while plate bending element has one out-of-plane translational degree of freedom and two rotational degrees of freedom. Although the in-plane rotational degree of freedom does not exist in the membrane element formulation, it can appear after the co-ordinate transformation from local to global [2]. If all elements sharing a node are coplanar, the absence of the in-plane rotational degree of freedom leads to zero values in the stiffness matrix and therefore results in the numerical singularity problem [1-3].

There have been two membrane elements proposed for tackling the singularity issue, which are the constant strain triangular (CST) and Allman triangular (AT) elements. The CST element assumes the stiffness for in-plane rotational degree of freedom [1-6]. On the other hand, the AT element is a higher order membrane element including the in-plane rotational degree of freedom [7-9]. In this work, the performances of the CST and AT elements have been compared. Both membrane elements were combined with the widely-used discrete Kirchhoff triangular (DKT) plate bending element [10] to solve several plate structural problems.

2. Governing Equations

The governing equations for the in-plane deformation and transverse deflection of a plate lying in a local *x-y* coordinate system are briefly described in this section.

2.1 In-Plane Deformation

The in-plane deformation is governed by the two-dimensional equilibrium equations [11]:

$$\frac{\partial \sigma_x}{\partial x} + \frac{\partial \tau_{xy}}{\partial y} + F_x = 0 \qquad (1)$$

and

$$\frac{\partial \tau_{xy}}{\partial x} + \frac{\partial \sigma_y}{\partial y} + F_y = 0 \qquad (2).$$

The stress components σ_x , σ_y and τ_{xy} are related to the strain components by Hooke's law:

$$\{\sigma\} = [C]\{\varepsilon\} \qquad (3)$$

where $\{\sigma\}$ and $\{\varepsilon\}$ are defined by:

$$\{\sigma\}^T = \lfloor \sigma_x \quad \sigma_y \quad \tau_{xy} \rfloor \qquad (4)$$

and

$$\{\varepsilon\}^T = \left\lfloor \frac{\partial u}{\partial x} \quad \frac{\partial v}{\partial y} \quad \frac{\partial u}{\partial y} + \frac{\partial v}{\partial x} \right\rfloor \qquad (5).$$

For plane stress problem, the material stiffness matrix $[C]$ is:

$$[C] = \frac{E}{1-\nu^2}\begin{bmatrix} 1 & \nu & 0 \\ \nu & 1 & 0 \\ 0 & 0 & (1-\nu)/2 \end{bmatrix} \qquad (6).$$

2.2. Transverse Deflection

The transverse deflection w in *z*-direction normal to the *x-y* plane of a thin plate is given by the equilibrium equation [12]:

$$D\left(\frac{\partial^4 w}{\partial x^4} + \frac{2\partial^4 w}{\partial x^2 \partial y^2} + \frac{\partial^4 w}{\partial y^4}\right) = p(x,y) \qquad (7)$$

where $p(x,y)$ is the applied lateral load normal to the plate and D is the bending rigidity defined by:

$$D = \frac{Et^3}{12(1-\nu^2)} \qquad (8)$$

where E is Young's modulus, ν is Poisson's ratio and t is thickness of the plate.

3. Finite Element Derivation

The FEM derivation for plate analysis by using the two element combinations, CST+DKT and AT+DKT, is presented in this section.

3.1 Constant Strain Triangle (CST)

The three-node CST element assumes a linear displacement distribution over the element. The FEM equations can be derived by applying the method of weighted residuals to the governing differential equations for the in-plane deformation, Eqs. (1) and (2), leading to the FEM equations in the form:

$$[K_m]\{\delta_m\} = \{F_m\} \tag{9}$$

where the vector $\{\delta_m\}$ contains the element nodal unknowns of the in-plane displacements in *x* and *y* directions. There are two in-plane displacements (*u* and *v*) per node, i.e. six unknowns per element.

The element stiffness matrix $[K_m]$ in Eq. (9) is defined by:

$$[K_m] = [B_m]^T [C_m][B_m]tA \tag{10}$$

where the strain-displacement interpolation matrix $[B_m]$ is given in Ref. [11]. The vector $\{F_m\}$ on the right-hand-side of Eq. (9) contains the applied mechanical forces at element nodes in *x* and *y* directions.

3.2 Allman Triangle (AT)

The three-node AT element is a plane triangular element with two displacements and one rotation at each corner as shown in Fig. 1(a). In the element, the tangential and normal displacements u_t and u_n along the side of the triangle are assumed to have linear and quadratic distribution, respectively [7]. For example, along edge 1-2, edge-tangent displacement is:

$$u_t = \left(1 - \frac{s}{L_3}\right) u_{t1} + \frac{s}{L_3} u_{t2} \tag{11}$$

where L_3 is the length of edge 1-2 and the edge-normal displacement is:

$$u_n = \left(1 - \frac{s}{L_3}\right) u_{n1} + \frac{s}{L_3} u_{n2} + \frac{4s}{L_3}\left(1 - \frac{s}{L_3}\right) u_{n12} \qquad (12).$$

The mid-edge normal displacement is relative to the straight-edge condition:

$$u_{n12} = \frac{L_3}{8}(\theta_{z2} - \theta_{z1}) \tag{13}$$

where θ_{z1} and θ_{z2} are in-plane nodal rotations. Considering the area coordinates of triangle [2], the element displacements along *x* and *y* directions are:

$$u = u_1\zeta_1 + u_2\zeta_2 + u_3\zeta_3 + 4u_{n12}\cos\theta_3\zeta_1\zeta_2 + 4u_{n23}\cos\theta_1\zeta_2\zeta_3 + 4u_{n31}\cos\theta_2\zeta_3\zeta_1 \tag{14}$$

and

$$v = v_1\zeta_1 + v_2\zeta_2 + v_3\zeta_3 + 4u_{n12}\sin\theta_3\zeta_1\zeta_2 + 4u_{n23}\sin\theta_1\zeta_2\zeta_3 + 4u_{n31}\sin\theta_2\zeta_3\zeta_1 \tag{15}$$

where θ_i is the angle between the *x* axis and the outward normal to the edge of length L_i. From the displacement fields in Eqs. (14) and (15), the Allman triangle element stiffness matrix can be constructed.

Considering the six-node linear strain triangle element (LST) [2] in Fig. 1(b), the displacements in x and y directions of node 4 can be written as:

$$u_4 = \frac{1}{2}u_1 + \frac{1}{2}u_2 - \frac{y_{12}}{8}(\theta_{z2} - \theta_{z1}) \tag{16}$$

and

$$v_4 = \frac{1}{2}v_1 + \frac{1}{2}v_2 + \frac{x_{12}}{8}(\theta_{z2} - \theta_{z1}) \qquad (17).$$

For nodes 5 and 6, the expression of the displacements can be written in the same pattern. Therefore, the relation between the LST and the Allman triangle is

$$\{\delta_1\} = [T]\{\delta_2\} \tag{18}$$

where

$$\{\delta_1\} = \{u_1 \quad v_1 \quad u_2 \quad \cdots \quad u_6 \quad v_6\}^T \tag{19}$$

and

$$\{\delta_2\} = \{u_1 \quad v_1 \quad \theta_{z1} \quad \cdots \quad u_3 \quad v_3 \quad \theta_{z3}\} \qquad (20).$$

$[T]$ is the 12x9 transformation matrix described in Ref. [13]. Consequently, the stiffness matrix of the Allman triangle can be obtained from the stiffness matrix of the LST triangle by the relationship:

$$[k_A] = [T]^T [k_{LST}][T] \qquad (21).$$

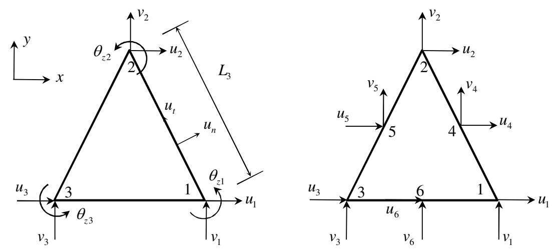

(a) (b)

Fig. 1 (a) The Allman triangular element.

(b) The linear strain triangular element.

3.3 Discrete Kirchoff Triangle (DKT)

The DKT element assumes a cubic distribution of the transverse deflection over the element [10]. The FEM derivation can be carried out by applying the method of weighted residuals to the governing equation for the transverse deflection, Eq. (7), leading to:

$$[K_b]\{\delta_b\} = \{F_b\} \tag{22}$$

where the vector $\{\delta_b\}$ contains the element nodal unknowns of the transverse deflections and rotations.

Each node has a transverse deflection in *z*-direction and two rotations about *x* and *y* directions, which are w, θ_x and θ_y, respectively. Therefore, there are nine degrees of freedom per element. The element stiffness matrix $[K_b]$ and the nodal force vector due to the applied lateral loads $\{F_b\}$ are defined by:

$$[K_b] = \int_A [B_b]^T [D][B_b]\, dA \tag{23}$$

and

$$\{F_b\} = \int_A [N_b]^T p\, dA \tag{24}$$

where the strain-displacement interpolation matrix $[B_b]$ is:

$$[B_b] = \frac{1}{2A}\begin{bmatrix} y_{31}\left[\dfrac{\partial H_x}{\partial \xi}\right] + y_{12}\left[\dfrac{\partial H_x}{\partial \eta}\right] \\ -x_{31}\left[\dfrac{\partial H_y}{\partial \xi}\right] - x_{12}\left[\dfrac{\partial H_y}{\partial \eta}\right] \\ -x_{31}\left[\dfrac{\partial H_x}{\partial \xi}\right] - x_{12}\left[\dfrac{\partial H_x}{\partial \eta}\right] + y_{31}\left[\dfrac{\partial H_y}{\partial \xi}\right] + y_{12}\left[\dfrac{\partial H_y}{\partial \eta}\right] \end{bmatrix} \tag{25}$$

where $\left\{\dfrac{\partial H_x}{\partial \xi}\right\}$, $\left\{\dfrac{\partial H_x}{\partial \eta}\right\}$, $\left\{\dfrac{\partial H_y}{\partial \xi}\right\}$ and $\left\{\dfrac{\partial H_y}{\partial \eta}\right\}$ are given in Ref [10]. The closed-form FEM matrices directly used for computer programming are described in Ref [14].

3.4 In-plane rotation stiffness

The FEM equation for flat shell element can be written in the form:

$$[K]^{(ele)}\{\delta\}^{(ele)} = \{F\}^{(ele)} \tag{26}$$

The unknown vector matrix $\{\delta\}^{(ele)}$ consists of six degrees of freedom (i.e., $u, v, w, \theta_x, \theta_y$, and θ_z) per node. For the combination of CST and DKT elements, the element stiffness matrix for each node, $K_i^{(ele)}$, which is the superposition of $[K_m]$ and $[K_b]$ from Eqs. (10) and (23) can be written as:

$$K_i^{(ele)} = \begin{bmatrix} [K_{mi}]_{2\times 2} & [0]_{2\times 3} & 0 \\ [0]_{3\times 2} & [K_{bi}]_{3\times 3} & 0 \\ 0 & 0 & 0 \end{bmatrix} \tag{27}$$

The element stiffness matrix contains zero values of the stiffness corresponding to the in-plane rotational degree of freedom, θ_z (or drilling degree of freedom [1]). If any node is surrounded by coplanar elements, the stiffness matrix becomes singular. To deal with this problem, the stiffness for the drilling degree of freedom is approximated as [1-2]:

$$K_{\theta_z i} = \alpha E A t \begin{bmatrix} 1 & -0.5 & -0.5 \\ -0.5 & 1 & -0.5 \\ -0.5 & -0.5 & 1 \end{bmatrix} \tag{28}$$

where E is Young's modulus, A is element area, t is element thickness and α is an arbitrarily chosen number (10^{-5} for the present study).

4. Numerical Evaluation

Three numerical examples were used to evaluate the performances of the two element combinations, CST+DKT and AT+DKT.

4.1 Pure Bending of Square Plate

The 2x2 m^2 square plate in Fig. 2 is subjected to the load T_x along left and right edges with the amplitude of σ_0 = 100 Pa [7]. The Young's modulus, Poisson's ratio, and thickness of the plate are 190 GPa, 0.3, and 0.01 m respectively. The load T_x varies along *y* direction as:

$$T_x = 2\left(\frac{y}{L}\right)\sigma_0 \tag{29}$$

For this problem, the exact solutions of the in-plane displacement are [7]:

$$u = 2\left(\frac{\sigma_0}{E}\right)\frac{xy}{L} \tag{30}$$

and

$$v = -\left(\frac{\sigma_0}{E}\right)\frac{x^2 + \nu y}{L} \tag{31}$$

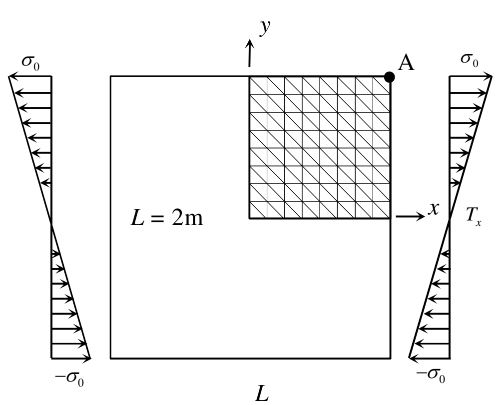

Fig. 2 Pure bending of a square plate.

Since the problem is symmetrical, a quarter of the plate was modeled as depicted in Fig. 2. The plate is modeled by uniform mesh of 2x2 (9 nodes), 4x4 (25 nodes), 8x8 (81 nodes) and 10x10 (121 nodes) intervals. Figs. 3 and 4 show the computed displacements in *x* and *y* directions along the top edge by using 121 nodes. The results suggest that both CST+DKT and AT+DKT element combinations give accurate displacement values at this mesh size.

Figs. 5 and 6 show the calculated displacements at position A in Fig. 2 in *x* and *y* directions, respectively. The numerical results are closer to the exact solutions when node number increases. It is noticeable that the solution accuracy of the AT+DKT element combination is slightly better than that of the CST+DKT (Figs. 5 and 6). This can be attributed to the fact that the order of interpolation function of the AT element is higher than that of the CST element.

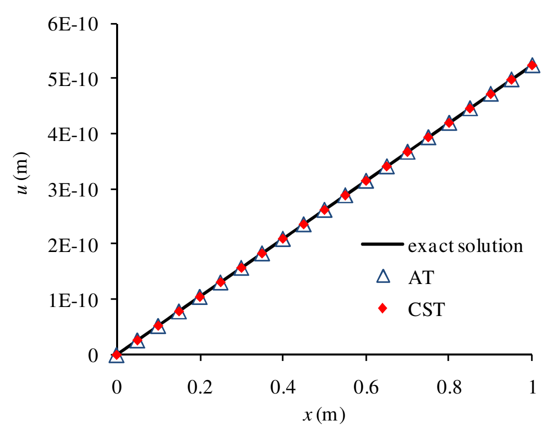

Fig. 3 Result comparison for the displacement in *x*-direction along the top edge.

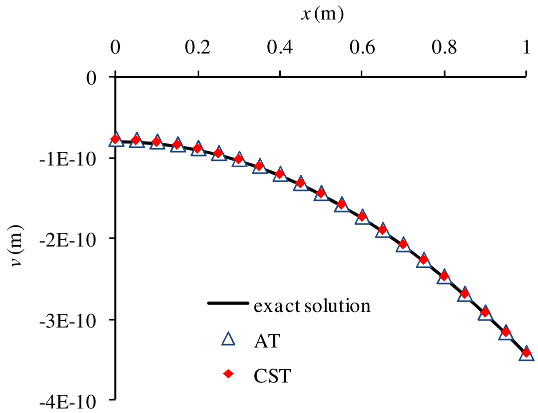

Fig. 4 Result comparison for the displacement in *y*-direction along the top edge.

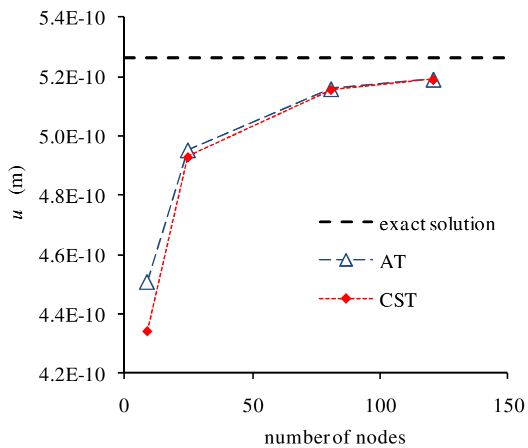

Fig. 5 Result comparison for the displacement in *x*-direction at point A in Fig. 2.

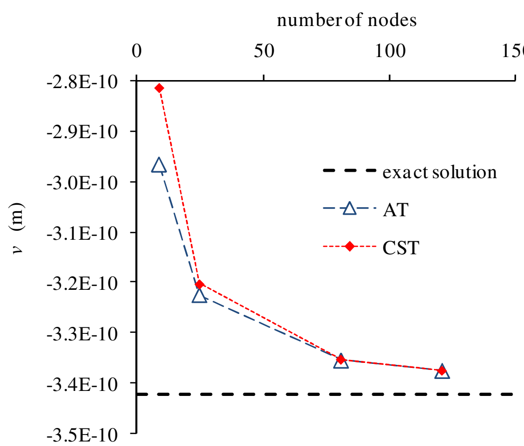

Fig. 6 Result comparison for the displacement in *y*-direction at point A in Fig. 2.

4.2 Cylindrical Shell

The cylindrical shell in Fig. 7 is subjected to the point load *P* of 100 N [15]. The shell has the length *L* of 10.35 m, radius *R* of 4.953 m, thickness of 0.094 m, Young's modulus of 10.5×10^6 N/m^2 and Poisson's ratio of 0.3125. Due to the geometrical symmetry, only one eighth of the cylinder was modeled as illustrated in Fig. 8. Four mesh sizes, which are 2x2 (9 nodes), 4x4 (25 nodes), 8x8 (81 nodes) and 10x10 (121 nodes), were used for mesh sensitivity study.

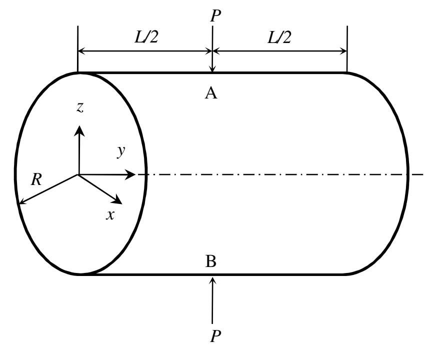

Fig. 7 Cylindrical shell under a point load.

Fig. 9 shows the computed displacement values in *z*-direction at point A compared to the exact solution. The numerical results are closer to the exact solution with increasing node number. In this problem, the CST+DKT and AT+DKT element combinations give similar *z*-direction displacement for every mesh size used.

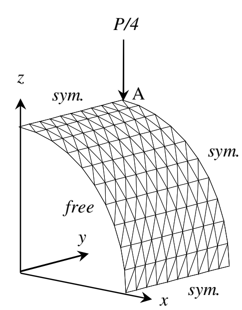

Fig. 8 FEM model of the cylindrical shell problem in Fig. 7.

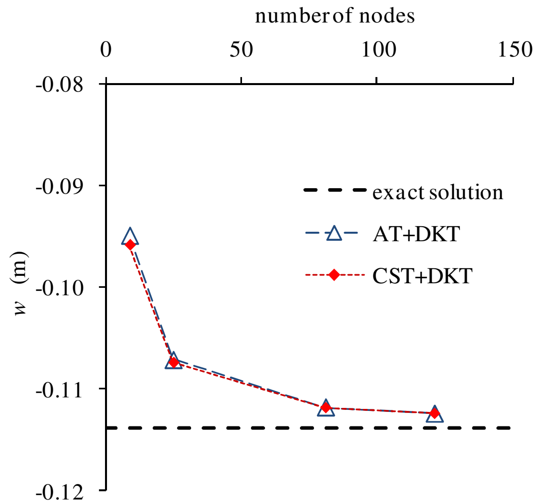

Fig. 9 Result comparison for the displacement in *z*-direction at point A in Fig. 7.

4.3 Pinched Hemispherical Shell

Fig. 10 shows a hemispherical shell with a 18° hole on the top subjected to two pairs of equal (F = 2 N) but opposite concentrated loads (applied in the z=0 plane and along x and y axes) [15]. This numerical example was commonly used to test the problem of membrane locking of shell elements [15]. The hemispherical shell has the radius R of 10 m, thickness of 0.04 m, Young's modulus of 6.825×10^7 N/m^2 and Poisson's ratio of 0.3.

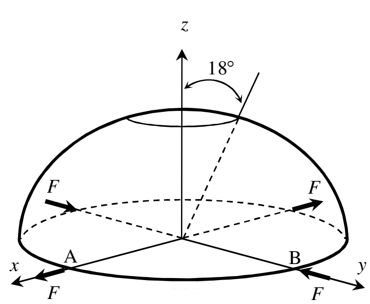

Fig. 10 Pinched hemispherical shell.

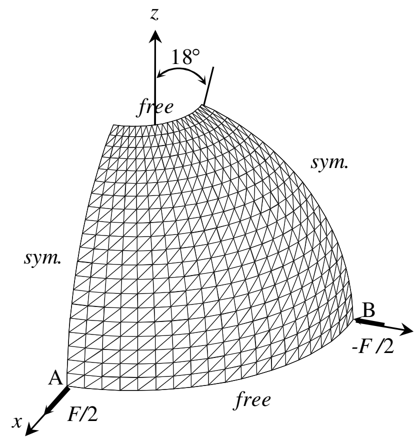

Fig. 11 FEM Model of the pinched hemispherical shell problem in Fig. 10.

Only a quarter of the shell can be modeled due to its symmetry, as illustrated in Fig. 11. To check mesh sensitivity, six mesh sizes were used, which are 10x10 (121 nodes), 16x16 (289 nodes), 20x20 (441 nodes), 24x24 (625 nodes), 32x32 (1089 nodes) and 40x40 (1681 nodes). Fig. 12 shows the calculated displacement values in x-direction at point A compared to the exact solution. The CST+DKT element combination gives acceptable solution accuracy in every mesh size used. On the other hand, solutions from the AT+DKT element combination are relatively far from the exact solution when using 121 and 289 nodes. This can be attributed to the problem of membrane locking. However, the effect of membrane locking seems to disappear when finer mesh was used. At 1089 and 1681 nodes, the CST+DKT and AT+DKT element combinations give similar x-direction displacement solutions.

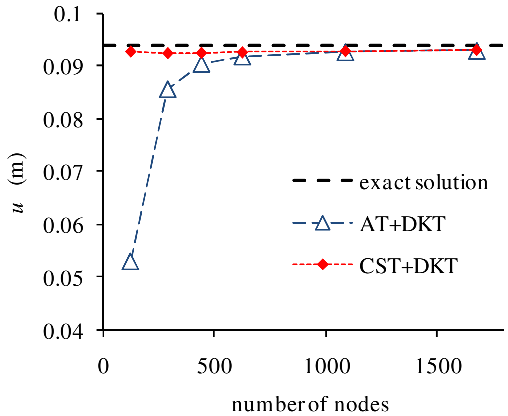

Fig. 12 Result comparison for the displacement in *x*-direction at point A in Fig. 10.

5. Conclusions

The performances of the CST+DKT and AT+DKT element combinations in plate structural analysis have been compared. Both element combinations give acceptable numerical solutions in most cases if FEM mesh is sufficiently fine. The results suggest that the solution from the AT+DKT element combination is slightly more accurate than that from the CST+DKT element. This is probably due to the fact that the interpolation function of the AT element has a higher order than that of the CST element. However, the use of the AT+DKT element combination could experience membrane locking problem in some cases at relatively coarse mesh.

6. Acknowledgements

This work is financially supported by National Metal and Materials Technology Center (MTEC).

7. References

[1] Zienkiewicz, O.C. and Taylor, R.L. (2005). The Finite Element Method for Solid and Structural Mechanics, 6th edition, Elsevier Butterworth-Heinemann, Oxford.

[2] Cook, R.D., Malkus, D.S., Plesha, M.E. and Witt, R.J. (2002). Concepts and Applications of Finite Element Analysis, John Wiley & Sons, New York.

[3] Yang, H.T.Y., Saigal, S., Masud, A. and Kapania, R.K. (2000). A survey of recent shell finite elements, *International Journal for Numerical Methods in Engineering*, vol.47(1-3), January 2000, pp. 101 – 127.

[4] Bathe, K.J. and Ho, L.W. (1981). A simple and effective element for analysis of general shell structures, *Computers and Structures*, vol.13(5-6), October–December 1981, pp. 673 – 681.

[5] Knight, N.F. Jr. (1997). Raasch challenge for shell elements, *AIAA Journal*, vol.35(2), February 1997, pp. 375 – 381.

[6] Nguyen-Thanh, N., Rabczuk, T., Nguyen-Xuan and Bordas, S.P.A. (2008). A smoothed finite element method for shell analysis, *Computer Methods in Applied Mechanics and Engineering*, vol.198(2), December 2008, pp. 165 – 177.

[7] Allman, D.J. (1984). A compatible triangular element including vertex rotations for plane elasticity analysis, *Computers and Structures*, vol.19(1-2), 1984, pp. 1 – 8.

[8] Bergan, P.G. (1985). A triangular membrane element with rotational degrees of freedom, *Computer Methods in Applied Mechanics and Engineering*, vol.50(1), July 1985, pp. 25 – 69.

[9] Hughes, T.J.R., Masud, A. and Harari, I. (1995). Numerical assessment of some membrane elements with drilling degrees of freedom, *Computers and Structures*, vol.55(2), April 1995, pp. 297 – 314.

[10] Batoz, J.L., Bathe, K.J. and Ho, L.W. (1980). A study of three-node triangular plate

bending elements, *International Journal for Numerical Methods in Engineering*, vol.15(12), December 1980, pp. 1771 – 1812.

[11] Dechaumphai, P. (2010). Finite Element Method: Fundamentals and Applications, 1st edition, Alpha Science International, Oxford.

[12] Timoshenko, S. and Krieger, S.W. (1970). Theory of Plates and Shells, 3rd edition, McGraw-Hill, Singapore.

[13] Cook, R.D. (1986). On the Allman triangle and a related quadrilateral element, *Computers and Structures*, vol.22(6), 1986, pp. 1065 – 1067.

[14] Jeyachandrabose, C., Kirkhope, J. and Babu, C.R. (1985). An alternative explicit formulation for the DKT plate-bending element, *International Journal for Numerical Methods in Engineering*, vol.21(7), July 1985, pp. 1289 – 1293.

[15] Wanji, C. and Cheung, Y.K. (1999). Refined non-conforming triangular elements for analysis of shell structures, *International Journal for Numerical Methods in Engineering*, vol.46(3), September 1999, pp. 433 – 455.